Acta Biomaterialia 9 (2013) 7679–7690

Contents lists available at SciVerse ScienceDirect

Acta Biomaterialia

journal homepage: www.elsevier.com/locate/actabiomat

pH-sensitive micelles self-assembled from multi-arm star triblock co-polymers poly(ε-caprolactone)-b-poly(2-(diethylamino)ethyl methacrylate)-b-poly(poly(ethylene glycol) methyl ether methacrylate) for controlled anticancer drug delivery

You Qiang Yang [a], Bin Zhao [a], Zhen Dong Li [b], Wen Jing Lin [a], Can Yang Zhang [a], Xin Dong Guo [a], Ju Fang Wang [b], Li Juan Zhang [a,*]

[a] School of Chemistry and Chemical Engineering, South China University of Technology, Guangzhou 510640, People's Republic of China
[b] School of Bioscience and Bioengineering, South China University of Technology, Guangzhou 510640, People's Republic of China

ARTICLE INFO

Article history:
Received 24 January 2013
Received in revised form 22 April 2013
Accepted 2 May 2013
Available online 10 May 2013

Keywords:
Micelles
pH-responsive
Star co-polymer
Anticancer drug delivery

ABSTRACT

A series of amphiphilic 4- and 6-armed star triblock co-polymers poly(ε-caprolactone)-b-poly(2-(diethylamino)ethyl methacrylate)-b-poly(poly(ethylene glycol) methyl ether methacrylate) (4/6AS-PCL-b-PDEAEMA-b-PPEGMA) were developed by a combination of ring opening polymerization and continuous activators regenerated by electron transfer atom transfer radical polymerization. The critical micelle concentration values of the star co-polymers in aqueous solution were extremely low (2.2–4.0 mg l^{-1}), depending on the architecture of the co-polymers. The self-assembled blank and doxorubicin (DOX)-loaded three layer micelles were spherical in shape with an average size of 60–220 nm determined by scanning electron microscopy and dynamic light scattering. The in vitro release behavior of DOX from the three layer micelles exhibited pH-dependent properties. The DOX release rate was significantly accelerated by decreasing the pH from 7.4 to 5.0, due to swelling of the micelles at lower pH values caused by the protonation of tertiary amine groups in DEAEMA in the middle layer of the micelles. The in vitro cytotoxicity of DOX-loaded micelles to HepG2 cells suggested that the 4/6AS-PCL-b-PDEAEMA-b-PPEGMA micelles could provide equivalent or even enhanced anticancer activity and bioavailability of DOX and thus a lower dosage is sufficient for the same therapeutic efficacy. The results demonstrate that the pH-sensitive multilayer micelles could have great potential application in delivering hydrophobic anticancer drugs for improved cancer therapy.

1. Introduction

Due to the heterogeneity and adaptations of cancerous cells cancer therapy remains a tremendous challenge and great efforts have been devoted to cancer therapy over the past several decades. Chemotherapy plays an important role in cancer therapy and has become one of the most widely used tools in combating cancer. However, there are still various intrinsic limitations of anticancer agents, such as poor water solubility, uncontrolled pharmacokinetic processes (short duration in the circulation and improper biodistribution), and the possible occurrence of severe side-effects, which will considerably decrease the therapeutic efficacy [1–3].

Recently novel drug delivery approaches (e.g., nanoparticles, liposomes, hydrogels and polymeric micelles) have been investigated to obtain higher antitumor efficiency with reduced toxicity by altering the biodistribution of anticancer drugs [4–9]. In addition, nanoparticles with a hollow structure have also been attracting attention because they can encapsulate drugs with high efficacy [10–13]. Polymeric micelles with nanoscopic core–shell structures formed by amphiphilic co-polymers demonstrate a series of attractive properties as anticancer drug carriers, providing a high loading capacity of poorly water soluble drugs, improving the apparent water solubility, providing both passive and active targeting capabilities, altering the pathways of drug biocirculation, reducing uptake by the reticuloendothelial system (RES), prolonging the in vivo circulation duration and increasing specific accumulation within tumor tissues, thus affording enhanced therapeutic efficacy and negligible adverse effects [14–17].

However, the formation of polymeric micelles is thermodynamically favorable only above the critical micelle concentration (CMC) of the amphiphilic molecules and they are relatively unstable in infinitely dilute environments. Once introduced into the

* Corresponding author. Tel./fax: +86 20 87112046.
E-mail address: celjzh@scut.edu.cn (L.J. Zhang).

1742-7061/$ - see front matter © 2013 Acta Materialia Inc. Published by Elsevier Ltd. All rights reserved.
http://dx.doi.org/10.1016/j.actbio.2013.05.006

bloodstream by intravenous administration polymeric micelles become thermodynamically unstable when the concentration of amphiphilic polymers drops below the CMC by severe dilution. The disruption of micellar structures might lead to the burst release of physically encapsulated drugs, which may cause serious side-effects, mostly due to large fluctuations in the drug concentration [18,19]. All these characteristics may reduce the effectiveness of drug delivery and limit the in vivo application of polymeric micelles.

In contrast to the classical linear polymers, one promising approach to improving the thermodynamic stability of micelles is to develop star-shaped amphiphilic polymers which mimic the morphology of polymeric micelles. Star-shaped polymers, a form of dendritic polymer, present unique properties and advantages, such as a small hydrodynamic radius, a large number of arms, which are capable of forming a stable micelle structure, a low intrinsic viscosity and crystallinity, high functionality and simple synthesis, owing to their particular well-defined architecture with multiple polymer chains radiating from the central core [2,20–23]. Thus amphiphilic star-shaped co-polymers could be promising candidates for anticancer drug delivery [24–29].

Considering the tumor targeting drug delivery field, an ideal anticancer drug carrier should retain the drug molecules in the micellar core in the bloodstream and normal tissues and release them at the specific tumor sites. So the production of pH-responsive star polymers could significantly expand the application of these polymers [26,30–33]. Compared with the normal physiological environment of pH 7.4, the extracellular pH values in tumorous tissues have been determined to be around 6.5–7.0, and the intracellular pH of the endosomal and lysosomal environments is typically acidic (pH 5.0 and 4.5–5.0) [34–36]. Poly(2-(diethylamino)ethyl methacrylate) (PDEAEMA), a cationic polyelectrolyte with a pK_b of 6.9, making it soluble in acidic solution by protonation of the pendant amine groups but hydrophobic at around neutral pH, is a promising pH-sensitive material for tumor-targeted drug delivery [34,37]. Well-defined four arm poly(ethylene oxide)-b-poly(2-(diethylamino)ethyl methacrylate) (four arm PEO-b-PDEAEMA) has been synthesized and its pH-responsive self-assembly examined. The results showed that the micelles shrank due to electrostatic charge screening of the protonated DEAEMA groups at high pH and dissociated into unimers at low pH [38]. Furthermore, four arm PEO-b-PDEAEMA micelles possessed a high gene transfection efficiency for the delivery of DNA [39]. A co-micelle drug delivery system of a star block co-polymer poly(ε-caprolactone)-block-poly(diethylamino)ethyl methacrylate (S(PCL-b-PDEAEMA)) and a linear block cpolymer methoxy poly(ethylene glycol)-block-poly(ε-caprolactone) (mPEG-b-PCL) was developed to enhance the micelle stability and improve the pH-sensitive release behavior [40].

However, the relationship between the molecular structure of the star polymers and the drug release performance has still not been clearly elaborated and the drug delivery performance of these pH-sensitive star polymeric micelles was still far from satisfactory. Thus enhancing the accuracy of the response to a stimulus and the drug delivery effectiveness and bioavailability, and forming an integrated understanding of the mechanism of drug release from star polymeric micelles are imperative [41]. We herein report pH-sensitive three layer micelles self-assembled from amphiphilic 4- and 6-arm star triblock poly(ε-caprolactone)-b-poly(2-(diethylamino)ethyl methacrylate)-b-poly(poly(ethylene glycol) methyl ether methacrylate) (4/6AS-PCL-b-PDEAEMA-b-PPEGMA) for efficient intracellular anticancer drug delivery. These micelles have a hydrophobic poly(ε-caprolactone) (PCL) to encapsulate the anticancer drug, a pH-responsive middle poly(2-(diethylamino)ethyl methacrylate) (PDEAEMA) layer and a poly(ethylene glycol) (PEG) outer layer. The pH-responsive PDEAEMA layer is hydrophobic and collapses on the core at physiological pH (7.4), which can prevent premature burst drug release, but becomes highly positively charged by protonation of the pendant tertiary amine groups and leads to the micelles being adsorbed onto negatively charged cell membranes and subsequently endocytosed by tumor cells at tumor extracellular pH. Once internalized and transferred to lysosomes the further charged PDEAEMA leads to faster release of the entrapped drug into the cytoplasm and nucleus [34]. The hydrophilic PPEGMA with short side-chains, known to be non-immunogenic, non-antigenic and non-toxic, is distributed on the surface of the self-assembled micelles and provides a compact protective layer maintaining the stability of the micelles in the circulation [42,43]. Doxorubicin (DOX), one of the most potent anticancer drugs [44], was used as a model drug encapsulated in the 4/6AS-PCL-b-PDEAEMA-b-PPEGMA micelles. The influence of the PCL and PDEAEMA contents, and the 4- or 6-arm topological structure on the micellar physico-chemical properties and release performance, as well as the final anticancer activity, were explored in depth.

2. Materials and methods

2.1. Materials

ε-Caprolactone (ε-CL) (99% pure, Aldrich) was dried over calcium hydride and distilled under reduced pressure before use. 2-(Diethylamino)ethyl methacrylate (DEAEMA) (TCI-EP) was distilled from calcium hydride, and stored under argon at −20 °C. Poly(ethylene glycol) methyl ether methacrylate (PEGMA) (M_n 475 Da, 99% pure, Aldrich) was purified by passage through a column filled with neutral alumina to remove inhibitor. Pentaerythritol and dipentaerythritol was dried under reduced pressure overnight prior to use. Tetrahydrofuran (THF) was dried over sodium using benzophenone as a dryness indicator and distilled under nitrogen prior to use. Toluene was distilled from calcium hydride. Pyrene (99% pure Aldrich), 2-bromoisobutyryl bromide (98% pure, Alfa Aesar), 1,1,4,7,10,10-hexamethyltriethylenetetramine (HMTETA) (99% pure, Aldrich), $CuBr_2$, methanol, stannous octoate ($Sn(Oct)_2$), triethylamine (TEA), dimethyl sulfoxide (DMSO), acetone, and all other reagents were used as received. Doxorubicin hydrochloride (DOX·HCl) was purchased from Wuhan Yuancheng Gongchuang Technology Co. Ltd and used as received. Dulbecco's modified Eagle's medium (DMEM), fetal bovine serum (FBS), penicillin and streptomycin were all purchased from Invitrogen. HepG2 cells were purchased from the American Type Culture Collection (ATCC) and cultured under the recommended conditions according to the supplier. 3-(4,5-Dimethyltlliazol-2-yl)-2,5-diphenyltetrazoxium bromide (MTT) was purchased from Sigma Chemical Co.

2.2. Measurements

The number average molecular weight (M_n) and polydispersity index (M_w/M_n) were determined by gel permeation chromatography (GPC) using an Agilent 1200 series GPC system equipped with a LC quant pump, 5 μm PL-Gel™ 500 Å, 10,000 Å and 100,000 Å pore size columns in series, and a refractive index detector. The column system was calibrated with a set of monodisperse polystyrene standards using HPLC grade THF as the mobile phase with a flow rate of 1.0 ml min^{-1} at 30 °C. ^1H NMR spectra were recorded in *d*-$CDCl_3$ at 25 °C using a Bruker Avance III 400 operating at 250 MHz. Fluorescence spectra were obtained using a F-4500 fluorescence spectrophotometer (Hitachi, Japan). The micelle size and distribution (PDI) were determined by dynamic light scattering (DLS) (Malvern Zetasizer Nano S, Malvern, UK). The zeta potentials

were determined by electrophoretic measurement carried out with the same Malvern Zetasizer Nano S instrument. The measurements were performed three times for each sample at 25 °C. The morphologies of the micelles were investigated by scanning electron microscopy (SEM) (Leo 1530 VP, Germany).

2.3. Synthesis of 4/6AS-PCL-b-PDEAEMA-b-PPEGMA co-polymers

4/6AS-PCL-b-PDEAEMA-b-PPEGMA were synthesized by ring opening polymerizations (ROP) of ε-CL using pentaerythritol or dipentaerythritol as initiator, followed by continuous activator regenerated by electron transfer atom transfer radical polymerization (AGERT ATRP) of DEAEMA and PEGMA. As an example the typical synthesis procedure of 4AS-PCL-b-PDEAEMA-b-PPEGMA was as follows.

The initiator pentaerythritol (0.136 g, 1 mmol) was placed in a flame dried 100 ml Schlenk flask with a magnetic stirring bar. The flask was then evacuated and flushed three times with argon. Subsequently the freshly distilled ε-CL (12 g) and the required amount of $Sn(Oct)_2$ (0.1 wt.% ε-CL, 0.012 g) solution in 30 ml toluene were added in turn by syringe and the flask was immersed into a thermostat controlled oil bath at 100 °C. After 24 h the mixture was dissolved in approximately 50 ml THF, followed by dropwise addition to 500 ml water/methanol (50:50 vol.%) mixture. The precipitate was collected and dried under vacuum for 24 h, resulting in powdery 4AS-PCL-OH.

The hydroxyl group of 4AS-PCL-OH was then acylated by 2-bromoisobutyryl bromide. 4AS-PCL-OH (0.8 mmol) was added to a 250 ml flask with a magnetic stirring bar. The flask was evacuated and flushed three times with argon. Then anhydrous THF (150 ml) and TEA (2.22 ml, 16 mmol) were added in turn. After the solution had been cooled to 0 °C in an ice/water bath 2-bromoisobutyryl bromide (1.98 ml, 16 mmol) was added dropwise with vigorous stirring. The mixture was stirred at 0 °C for 5 h and then at room temperature for 24 h. The solution was passed through a neutral alumina column to remove quaternary ammonium salts, and then precipitated by water/methanol (50:50 vol.%) mixture. The final white powder product 4AS-PCL-Br was obtained after vacuum drying for 24 h.

Continuous ARGET ATRP of DEAEMA and PEGMA was monitored in situ using a ReactIR iC10 (Metter-Toledo AutoChem) equipped with a light conduit and DiComp (diamond composite) insertion probe. Fourier transform infrared (FTIR) spectra were collected every 1 min and the change in absorbance at 938 cm^{-1} (=CH_2 wags of DEAEMA and PEGMA) was used to calculate the degree of polymerization using the ReactIR 4.1 software. In brief, $CuBr_2$ (0.018 g, 0.08 mmol) and the macroinitiator 4AS-PCL-Br (0.4 mmol) were added to a dry 100 ml three-necked flask with a magnetic stirring bar. A real time FTIR probe was placed in the flask and the flask was then evacuated and flushed three times with argon. Anhydrous toluene (18 ml), DEAEMA (3.6 g) and ligand HMTETA (0.22 ml, 0.8 mmol) were introduced in turn into the flask using degassed syringes. The mixture was stirred for 10 min and a required amount of $Sn(Oct)_2$ (0.324 g, 0.8 mmol) solution in toluene (2 ml) was added to the flask by syringe. The flask was placed in a preheated oil bath maintained at 70 °C and FTIR spectra were collected. After 7 h the absorbance at 938 cm^{-1} was close to 0 and the second monomer PEGMA (M_n = 475, 3.6 g) was then added by syringe to continue the polymerization for another 8 h. Then the flask was removed from the oil bath and cooled to room temperature. THF (50 ml) was added to the flask and the mixture was then passed through a neutral alumina column to remove the catalyst. Finally, 4AS-PCL-b-PDEAEMA-b-PPEGMA was recovered by precipitation in a 10-fold excess of n-hexane, filtering, and drying under vacuum for 24 h.

2.4. CMC measurement

The CMC values of 4/6AS-PCL-b-PDEAEMA-b-PPEGMA were determined by the fluorescence probe technique using pyrene as the fluorescence probe. The 4/6AS-PCL-b-PDEAEMA-b-PPEGMA was first dissolved in deionized water and then diluted to a series of concentrations from 0.0001 to 0.1 mg ml^{-1} with deionized water. Then 10 ml polymer solution was added to the pyrene filled vials and the combined solution was equilibrated at room temperature in the dark for 48 h before measurement. The final concentration of pyrene was 6×10^{-7} M. The fluorescence excitation spectra of the polymer/pyrene solutions were measured and used to determine the CMC value.

2.5. Preparation of DOX-loaded micelles

The blank and DOX-loaded 4/6AS-PCL-b-PDEAEMA-b-PPEGMA self-assembled micelles were formed using the diafiltration method. DOX·HCl (0–20 mg) was stirred with a 2-fold excess of TEA (molar ratio) in 20 ml DMSO overnight to obtain DOX base. The 4/6AS-PCL-b-PDEAEMA-b-PPEGMA (40 mg) were dissolved in another 20 ml DMSO (40 ml for blank micelles) and then mixed with the DOX base solution, followed by stirring for 4 h. The solution was transferred to a dialysis bag and dialyzed against deionized water for 24 h at room temperature. The dialysate was filtered, lyophilized and the red powder produced stored at −20 °C until use. The size and morphology of the blank and DOX-loaded micelles were monitored by DLS and SEM.

The DOX loading content (LC) and entrapment efficiency (EE) were determined by UV/vis spectrophotometry (UV-2450, Shimadzu, Japan) at 480 nm. 1 mg of the DOX-loaded micelle powder was dissolved in 10 ml DMSO under vigorous vortexing. The concentration of DOX was calculated according to a standard curve of pure DOX/DMSO. The LC was defined as the weight ratio of entrapped DOX to that of the DOX-loaded micelles. The EE of DOX was obtained as the weight ratio between DOX incorporated in assembled micelles and that used in fabrication.

2.6. In vitro DOX release

The in vitro DOX release profiles from the 4/6AS-PCL-b-PDEAEMA-b-PPEGMA assembled micelles were evaluated using buffers with pH values of 5.0, 6.5 and 7.4. In a typical experiment 5 mg of DOX-loaded micelles was suspended in 5 ml phosphate-buffered saline (PBS) (pH 7.4 or 6.5) or acetate buffer (pH 5.0) and then placed in a dialysis bag (molecular weight cut-off 3500–4000). The whole bag was placed into 35 ml PBS or acetate buffer and shaken (100 r.p.m.) at 37 °C (RCZ-8B Dissolution Tester, TDTF, China). At specified time intervals 4 ml (V_e) samples were taken and an equal volume of fresh buffer added to maintain the total volume. The concentration of DOX in different samples was analyzed by UV/vis spectrophotometry at 480 nm. The cumulative percent drug release (E_r) was calculated using Eq. (1).

$$E_r(\%) = \frac{V_e \sum_1^{n-1} C_i + V_0 C_n}{m_{DOX}} \times 100 \quad (1)$$

where m_{DOX} represents the amount of DOX in the micelle, V_0 is the volume of the release medium (V_0 = 40 ml), and C_n represents the concentration of DOX in the nth sample. The in vitro release experiments were carried out in triplicate at each pH.

2.7. Dissipative particle dynamics (DPD) simulations

The coarse grained simulations were performed by the DPD method, which has been successfully applied in other drug delivery

systems [45] to investigate the pH sensitivity and drug distribution of drug-loaded 4/6AS-PCL-b-PDEAEMA-b-PPEGMA micelles (using 4AS-PCL-b-PDEAEMA-b-PPEGMA micelles as an example). In the DPD simulations the components comprised 3% DOX, 10% 4AS-PCL-b-PDEAEMA-b-PPEGMA micelles, and 87% water (by volume). Solution pH values of 7.4, 6.5 and 5.0 were used to investigate pH-induced effects on the drug-loaded micelles. The coarse grain models are shown in Scheme S1. The interaction parameters were calculated using Amorphous Cell and Discovery at 298.15 K in Materials Studio 5.0 (Accelrys Inc.) [46]. A cubic simulation box of $20 \times 20 \times 20\ r_c^3$ with periodic boundary conditions was applied in all three directions. The integration time step was 0.05 ns with 20,000 simulation steps.

2.8. Cell culture and cytotoxicity assay

The in vitro cytotoxicity of free DOX and blank and DOX-loaded 4/6AS-PCL-b-PDEAEMA-b-PPEGMA micelles were evaluated by the standard MTT assay against HepG2 cells. The HepG2 cells were first cultured in DMEM supplemented with 10% FBS, penicillin (100 U ml^{-1}), and streptomycin (100 μg ml^{-1}) at 37 °C in a CO_2 (5%) incubator for 3 days. For cytotoxicity assay HepG2 cells were seeded in a 96-well plate at an initial density of 1×10^4 cells per well in 200 μl of complete DMEM and allowed to grow for 24 h to reach 60–70% confluence. Free DOX and blank and DOX-loaded micelles solutions were prepared with DMEM medium at stock concentrations and then diluted to give various DOX and micelle concentrations. The medium in each well was replaced with 200 μl of pre-prepared sample solutions and the treated cells were incubated in 5% CO_2 at 37 °C for another 24 or 48 h. The cytotoxicity test was replicated in six wells. After replacing the samples with 180 μl of fresh medium and 20 μl of MTT solution (5 mg ml^{-1} in PBS buffer) the cells were further incubated for 4 h. The medium in each well was then removed and 200 μl of DMSO was added to dissolve the internalized purple formazan crystals. Finally, the plate was gently agitated for 15 min before the absorbance at 490 nm was recorded using a microplate reader (Multiskan Spectrum, Thermo Scientific, Finland). The relative cell viability (%) was determined by comparing the absorbance at 490 nm with control wells and calculated using Eq. (2).

$$\text{cell viability} = \frac{A_{\text{sample}} - A_{\text{blank}}}{A_{\text{control}} - A_{\text{blank}}} \times 100\% \quad (2)$$

where A_{control} and A_{sample} are the absorbance at 490 nm in the absence and presence of free DOX and the micelles, respectively, and A_{blank} is the absorbance at 490 nm without either cells or samples.

3. Results and discussion

3.1. Synthesis and characterization of 4/6AS-PCL-b-PDEAEMA-b-PPEGMA

The 4/6AS-PCL-b-PDEAEMA-b-PPEGMA were synthesized via ROP of ε-CL to produce 4- and 6-arm PCL, with subsequent continuous ARGET ATRP of DEAEMA and PEGMA as shown in Fig. 1 [47,48]. In the first step star-shaped hydroxyl-terminated poly(ε-caprolactone) (4/6AS-PCL) were synthesized using pentaerythritol (for 4AS-PCL) or dipentaerythritol (for 6AS-PCL) as initiators in the presence of a catalytic amount of $Sn(Oct)_2$ at 100 °C. Then the end hydroxyl groups of the 4/6AS-PCL were fully converted to bromine end-capped 4/6AS-PCL-Br by reaction with 2-bromoisobutyryl bromide in THF at room temperature. The 4/6AS-PCL-Br were then utilized as macroinitiators for the continuous ARGET ATRP of DEAEMA and PEGMA. The molar ratio of $Sn(Oct)_2$ to $CuBr_2$ was 10:1, i.e., a tiny amount of $CuBr_2$ catalyst used with a large excess of reducing agent $Sn(Oct)_2$ [49]. The reaction was carried out in toluene at 70 °C, in situ monitored by infrared spectroscopy (ReactIR) [50,51], and the conversion of DEAEMA and PEGMA during ARGET ATRP were calculated from the change in absorbance at 938 cm^{-1}.

After polymerization of DEAEMA had proceeded for 7 h conversion was approximately 1, and the second monomer PEGMA was added with continued polymerization for another 8 h until the conversion of PEGMA did not increase further (Fig. S1A). The first order kinetic plots for the continuous ARGET ATRP of DEAEMA and PEGMA showed straight lines (Fig. S1B), indicating that perfect control of the polymerization process had been achieved in the current work.

The molecular weights and chemical structures of the serial 4/6AS-PCL-b-PDEAEMA-b-PPEGMA (Table 1) were determined by GPC and ^1H NMR. All the GPC traces of the 4/6AS-PCL-b-PDEAEMA-b-PPEGMA showed a monomodal symmetric distribution, indicating a well-controlled process of continuous ARGET ATRP of DEAEMA and PEGMA (Fig. S2). The M_n and M_w/M_n values are listed in Table 1. It can be seen that the ratio M_w/M_n is below 1.5, which is acceptable for drug delivery applications.

Representative ^1H NMR spectra of 4/6AS-PCL-b-PDEAEMA-b-PPEGMA are depicted in Fig. 2. The signal at 4.06 ppm is ascribed to the $-CH_2O-$ groups of pentaerythritol and dipentaerythritol and the signals at 1.38, 1.65 and 2.31 ppm are the characteristic resonances of the $-CH_2-$ groups of the PCL backbone. The signals at 0.90 and 1.82–1.92 ppm are ascribed, respectively, to the $-CCH_3$ and $-CH_2-$ groups of the methacrylate backbone. The signals at 2.71 and 4.01 ppm are the characteristic resonances of the two co-terminous methylene protons of $-CH_2CH_2-$ in the DEAEMA unit, and the signals at 1.05 and 2.59 ppm belong, respectively, to the end methyl and methylene protons of $-CH_2CH_3$ in the DEAEMA unit. The characteristic PEG peaks of $-CH_2-$ and end-capped $-CH_3$ protons can be clearly seen at 3.66 and 3.40 ppm, respectively.

The degrees of polymerization of PCL (x), PDEAEMA (y) and PPEGMA (z) per arm were calculated from the integration ratio values of signal (d) to (a) (I_d/I_a), signal (m) to (d) (I_m/I_d) and signal (p) to (d) (I_p/I_d), respectively. The molecular weights ($M_{n,\ NMR}$) of 4/6AS-PCL-b-PDEAEMA-b-PPEGMA were also calculated from the integration ratios, and all the results are summarized in Table 1. The ^1H NMR results were almost consistent with the theoretical values, suggesting that well-defined 4/6AS-PCL-b-PDEAEMA-b-PPEGMA with different PCL/PDEAEMA/PPEGMA compositions were successfully synthesized and characterized.

3.2. CMC values of 4/6AS-PCL-b-PDEAEMA-b-PPEGMA

CMC values of 4/6AS-PCL-b-PDEAEMA-b-PPEGMA were estimated to confirm the formation of micelles. A lower CMC value is desirable as it increased the micelle stability in the bloodstream [2,19]. As the concentration of 4/6AS-PCL-b-PDEAEMA-b-PPEGMA increased the fluorescence intensity increased and the third peak in the excitation spectra of pyrene shifted from 336 to 339 nm. The CMC values were determined from the threshold concentration, where the intensity ratio I_{339}/I_{336} began to increase markedly, as shown in Fig. S3 [52]. The CMC values of 4/6AS-PCL-b-PDEAEMA-b-PPEGMA were determined to be 2.2–4.0 mg l^{-1}, and are listed in Table 1. Due to the extremely low CMC values, the micelles self-assembled from 4/6AS-PCL-b-PDEAEMA-b-PPEGMA could show good stability in solution, even after extreme dilution by the larger volume of the systemic circulation in the body [53].

It is known that a longer length of the hydrophobic block most likely lowers the overall CMC of co-polymers [54], so a polymer with a longer PCL length has a lower CMC. Thus the CMC of $4C_{34.5}D_{25.8}P_{4.4}$ (2.2 mg l^{-1}) was much lower than that of

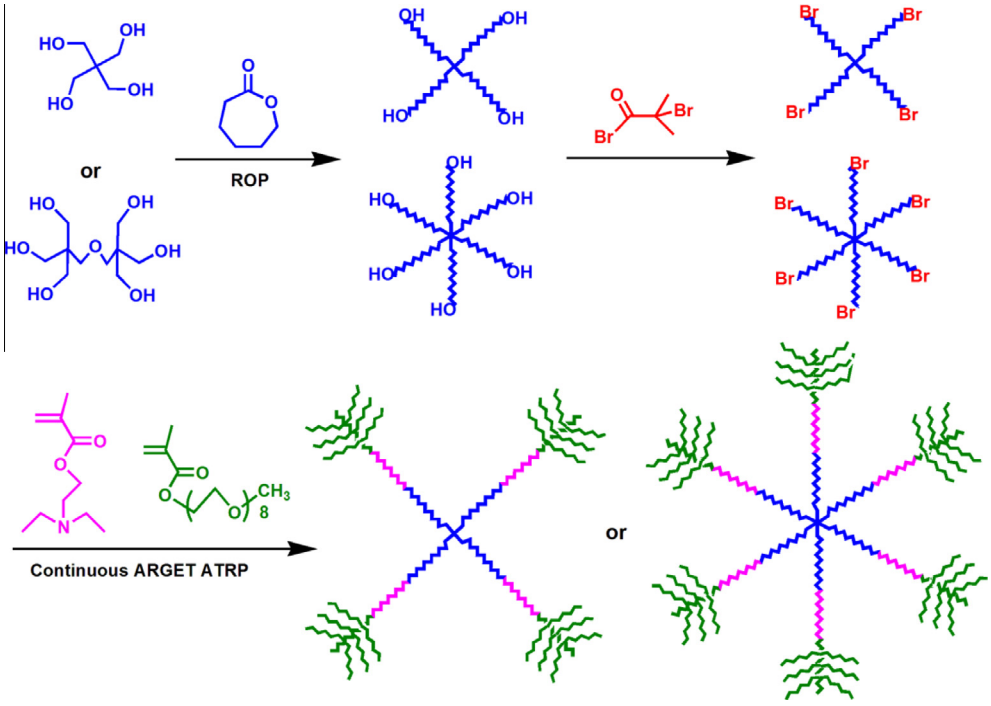

Fig. 1. Schematic description of the synthesis of 4/6AS-PCL-b-PDEAEMA-b-PPEGMA co-polymers.

Table 1
Characterization results of 4/6AS-PCL-b-PDEAEMA-b-PPEGMA co-polymers.

Polymer[a]	$M_{n,\ Th}$[b]	$M_{n,\ GPC}$[c]	M_w/M_n[c]	$M_{n,\ NMR}$[d]	CMC (mg l^{-1})
$4C_{22.2}D_{25.3}P_{4.9}$	39,000	33,385	1.45	38,887	3.8
$4C_{34.5}D_{14.5}P_{5.5}$	36,000	31,305	1.47	37,644	3.0
$4C_{34.5}D_{25.8}P_{4.4}$	45,000	43,321	1.36	43,916	2.2
$6C_{17.7}D_{8.5}P_{3.5}$	30,000	24,783	1.46	32,665	4.0
$6C_{17.7}D_{15.4}P_{3.4}$	39,000	33,295	1.39	40,039	3.8

[a] C, PCL; D, PDEAEMA; P, PPEGMA. The subscripts are the degree of polymerization of CL (x), DEAEMA (y) and PEGMA (z) calculated from the ^{1}H NMR spectra.
[b] Calculated by theory analysis from the feed ratio of monomers to initiator.
[c] Measured by GPC in THF.
[d] Calculated from the equations $M_{n,\ 4ASP} = (114 \times x + 185 \times y + 475 \times z + 149) \times 4 + 136$ and $M_{n,\ 6ASP} = (114 \times x + 185 \times y + 475 \times z + 149) \times 6 + 254$.

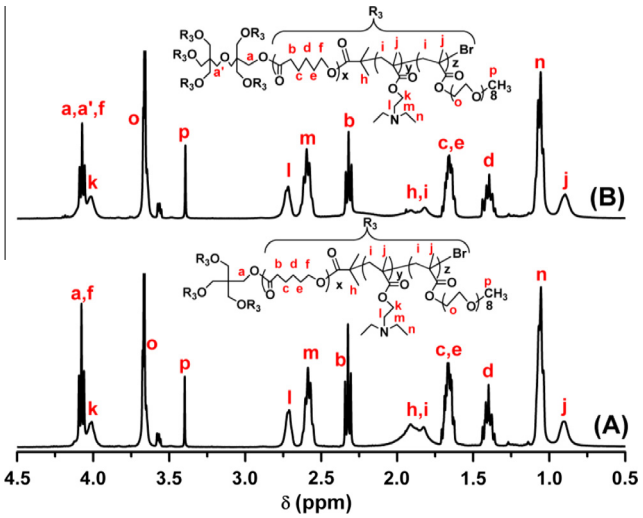

Fig. 2. ^{1}H NMR spectra of (A) 4AS-PCL-b-PDEAEMA-b-PPEGMA and (B) 6AS-PCL-b-PDEAEMA-b-PPEGMA in d-$CDCl_3$.

$4C_{22.2}D_{25.3}P_{4.9}$ (3.8 mg l^{-1}). Similarly, for the samples prepared with deionized water (pH 7.4) most tertiary amine residues of PDEAEMA remained deprotonated and were hydrophobic. Hence, for the same proportion of PCL moieties micellar formation of $4C_{34.5}D_{25.8}P_{4.4}$ required a weaker driving force, leading to a lower CMC of $4C_{34.5}D_{25.8}P_{4.4}$ (2.2 mg l^{-1}) compared with $4C_{34.5}D_{14.5}P_{5.5}$ (3.0 mg l^{-1}). The same trend can be seen for $6C_{17.7}D_{15.4}P_{3.4}$ (3.8 mg l^{-1}) and $6C_{17.7}D_{8.5}P_{3.5}$ (4.0 mg l^{-1}). Interestingly, the CMC of the 4- and 6-arm micelles with the same contents of PCL, PDEAEMA and PPEGMA moieties were equivalent in the current work, with $4C_{22.2}D_{25.3}P_{4.9}$ and $6C_{17.7}D_{15.4}P_{3.4}$ having the same CMC of 3.8 mg l^{-1}.

3.3. Characterization of the blank and DOX-loaded 4/6AS-PCL-b-PDEAEMA-b-PPEGMA micelles

The physico-chemical properties of the blank and DOX-loaded micelles were characterized by DLS analysis, as shown in Table 2. The average hydrodynamic diameters (D_h) of the blank micelles were below 150 nm, with a small polydispersity index (PDI $\leqslant$ 0.3). The micellar D_h values were greater than the theoretical D_h values of the unimers, which may be due to the fact that the 4/6AS-PCL-b-PDEAEMA-b-PPEGMA micelles were multimicelle aggregates rather than unimolecular micelles at a concentration of 1 mg ml^{-1}, which is apparently higher than th CMC values (2.2–4.0 mg l^{-1}). As is well known, at extremely low concentrations star co-polymers can form unimolecular micelles during primary aggregation. However, the unimolecular micelles spontaneously aggregate to form multimicelle aggregates at higher concentrations above the CMC [55]. Moreover, the longer length of the hydrophobic PCL block leads to enhanced hydrophobicity and a more convenient self-assembly process driven by hydrophobic interaction. The D_h of $4C_{34.5}D_{25.8}P_{4.4}$ micelles was larger (113.4 nm) than that of $4C_{22.2}D_{25.3}P_{4.9}M$ (76.8 nm). As most tertiary amine residues of PDEAEMA were still deprotonated and hydrophobic at pH 7.4, the micelles with longer length PDEAEMA blocks should have a larger hydrophobic core, resulting in an increase in D_h, such as for

Table 2
Hydrodynamic diameter (D_h), size distributions (PDI) and zeta potentials of blank and DOX-loaded 4AS-PCL-b-PDEAEMA-b-PPEGMA micelles.

Micelle	Blank			DOX-loaded		
	D_h (nm)	PDI	ζ Potential (mV)	D_h (nm)	PDI	ζ Potential (mV)
$4C_{22.2}D_{25.3}P_{4.9}M$	76.8	0.30	31.4	154.3	0.32	29.9
$4C_{34.5}D_{14.5}P_{5.5}M$	66.7	0.26	24.2	119.3	0.31	26.7
$4C_{34.5}D_{25.8}P_{4.4}M$	113.4	0.28	33.6	165.5	0.27	39.3
$6C_{17.7}D_{8.5}P_{3.5}M$	101.5	0.27	16.2	154	0.26	17.4
$6C_{17.7}D_{15.4}P_{3.4}M$	150.4	0.31	36.3	229	0.27	43.9

$4C_{34.5}D_{25.8}P_{4.4}M$ (113.4 nm) and $4C_{34.5}D_{14.5}P_{5.5}M$ (66.7 nm). However, as the spatial structure of 6AS-PCL-b-PDEAEMA-b-PPEGMA was extended compared with the 4 arm structure, the D_h of $6C_{17.7}D_{15.4}P_{3.4}M$ was greater than that of $4C_{22.2}D_{25.3}P_{4.9}M$, although they contained the same contents of PCL, PDEAEMA and PPEGMA moieties. The zeta potentials of the micelles shown in Fig. S4 were observed to be interconnected with the length of the PDEAEMA block polymers, and increased with increasing PDEAEMA length, such that the zeta potential of $4C_{34.5}D_{25.8}P_{4.4}M$ (33.6 mV) was higher than that of $4C_{34.5}D_{14.5}P_{5.5}M$ (24.2 mV) and the zeta potential of $6C_{17.7}D_{15.4}P_{3.4}M$ was 36.3 mV, compared with 16.2 mV for $6C_{17.7}D_{8.5}P_{3.5}M$. The zeta potentials of $4C_{34.5}D_{14.5}P_{5.5}M$ and $6C_{17.7}D_{15.4}P_{3.4}M$ were very close due to having the same PDEAEMA contents. The highly charged (16–36 mV) character of the micelles could prevent their aggregation, extend the blood circulation time, and increase the interaction between micelles and cell membranes, which could facilitate rapid penetration across the cell membrane [56,57].

After incorporation of DOX (feed ratio of DOX to polymer 20 or 40 mg) the average D_h of the DOX-loaded micelles increased ti approximately 50 nm compared with blank micelles, but was still below 230 nm. This can be attributed to fact that hydrophobic DOX promoted hydrophobic interaction among the PCL chains and thus led to an increase in aggregation. It is noteworthy that no obviouse changes in PDI and zeta potential were observed before and after DOX loading, suggesting that the small drug molecule had hardly any effect on the self-assembly of 4/6AS-PCL-b-PDEAEMA-b-PPEGMA micelles.

Fig. 3 presents SEM images of blank and DOX-loaded $4C_{34.5}D_{25.8}P_{4.4}M$. It can be seen that the micelles had a spherical morphology, both micelles being similar. Obviously, the D_h values seen in the SEM micrographs correspond to the multimicelle aggregates presented in Table 2. Co-polymer aggregation leads to multimolecular micelles, with sizes of the particles considerably higher than the maximum size that could have a multimolecular core–shell–corona micelle. The same spherical morphology was also observed for blank and DOX-loaded $6C_{17.7}D_{15.4}P_{3.4}M$, shown in Fig. S5.

The weight ratio of drug to polymer had a major influence on the LC and EE [15,58]. Table 3 illustrates the LC and EE values of DOX-loaded micelles. The LC increased with increasing fed drug for all DOX-loaded 4/6AS-PCL-b-PDEAEMA-b-PPEGMA micelles, while EE decreased for micellar cores with a saturated capacity to solubilize DOX. As discussed above, the hydrophobicity of the micellar core self-assembled from polymers with longer PCL block lengths was even stronger, suggesting an enhanced drug entrapping ability of the micelles, such that the LC of $4C_{34.5}D_{25.8}P_{4.4}M$ was 20.6%, compared with 10.4% for $4C_{22.2}D_{25.3}P_{4.9}M$ at a feed ratio 20/40. It is worth noting that increasing the length of the PDEAEMA block caused a slight decrease in LC, attributed to the partial protonation of DEAEMA, leading to mild attenuation of the hydrophobicity of DEAEMA and electrostatic repulsion between the DOX and PDEAEMA chains. On the other hand, the 6AS-PCL-b-PDEAEMA-b-PPEGMA micelles exhibited an enhanced drug entrapping ability compared with 4AS-PCL-b-PDEAEMA-b-PPEGMA micelles. This may be due to the enhanced spatial structure of the 6-arm micellar core compared with the 4-arm structure, and the larger core could accommodate even more drug. In the present work the maximum DOX LC and EE achieved were 20.6% and 60%, respectively.

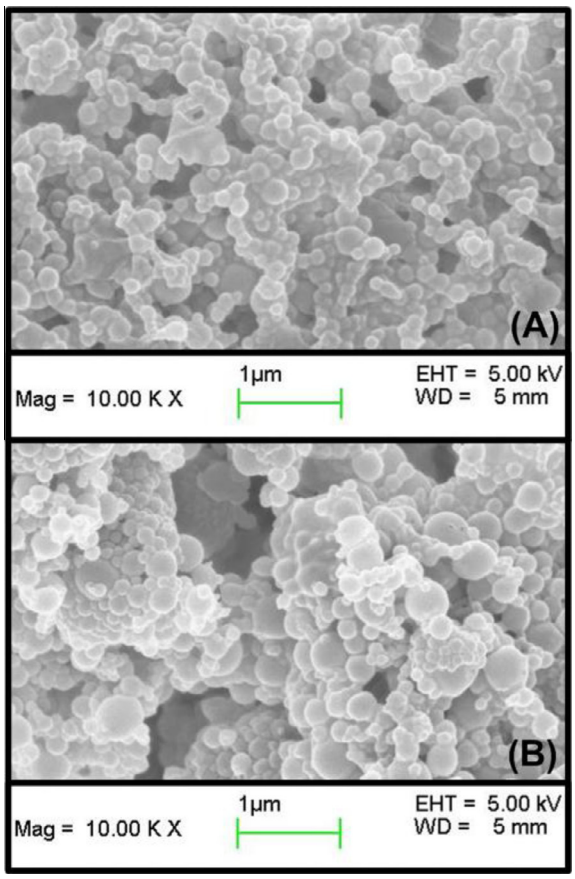

Fig. 3. SEM images of (A) blank and (B) DOX-loaded $4C_{34.5}D_{25.8}P_{4.4}M$.

Table 3
DOX loading content (LC) and entrapment efficiency (EE) of DOX-loaded 4AS-PCL-b-PDEAEMA-b-PPEGMA micelles.

Micelle	DOX/polymer	LC (%)	EE (%)
$4C_{22.2}D_{25.3}P_{4.9}M$	10/40	8.0	34.8
	20/40	10.4	23.2
$4C_{34.5}D_{14.5}P_{5.5}M$	10/40	12.0	54.5
	20/40	20.6	51.9
$4C_{34.5}D_{25.8}P_{4.4}M$	10/40	11.3	60.0
	20/40	17.6	42.7
$6C_{17.7}D_{8.5}P_{3.5}M$	10/40	9.7	43.0
	20/40	12.9	29.6
$6C_{17.7}D_{15.4}P_{3.4}M$	10/40	8.6	37.6
	20/40	11.7	26.5

3.4. In vitro drug release profiles and mechanism studies of DOX from 4/6AS-PCL-b-PDEAEMA-b-PPEGMA micelles

To evaluate the effects of pH-responsive behavior on controlled drug delivery the in vitro drug release profiles of DOX-loaded 4/6AS-PCL-b-PDEAEMA-b-PPEGMA micelles were determined under physiological condition (PBS, pH 7.4) and in a slightly acidic environment (pH 6.5 and 5.0), to simulate the pH of the endosomal and lysosomal microenvironments, as shown in Fig. 4. The release of DOX was pH dependent, and the release rate markedly accelerated as the pH decreased from 7.4 to 5.0. Under neutral conditions (pH 7.4), shown in Fig. 4A, only 10–18% of DOX was released in 6 h, and then the release rate was almost constant, owing to the tight structure of the micelles. Less than 40% of DOX was released in 48 h and about 50% after 108 h, which indicates that the drug is well protected with minimal DOX release from the micelles in the blood circulation, resulting in decreased toxicity to normal tissues. It can also be observed that the cumulative release of DOX from 6AS-PCL-b-PDEAEMA-b-PPEGMA micelles was much lower than from 4AS-PCL-b-PDEAEMA-b-PPEGMA micelles, with only 25% of DOX released in 108 h, mainly attributed to the highly entwined and compact micellar core of the 6AS-PCL-b-PDEAEMA-b-PPEGMA micelles, which can result in better entrapment of DOX.

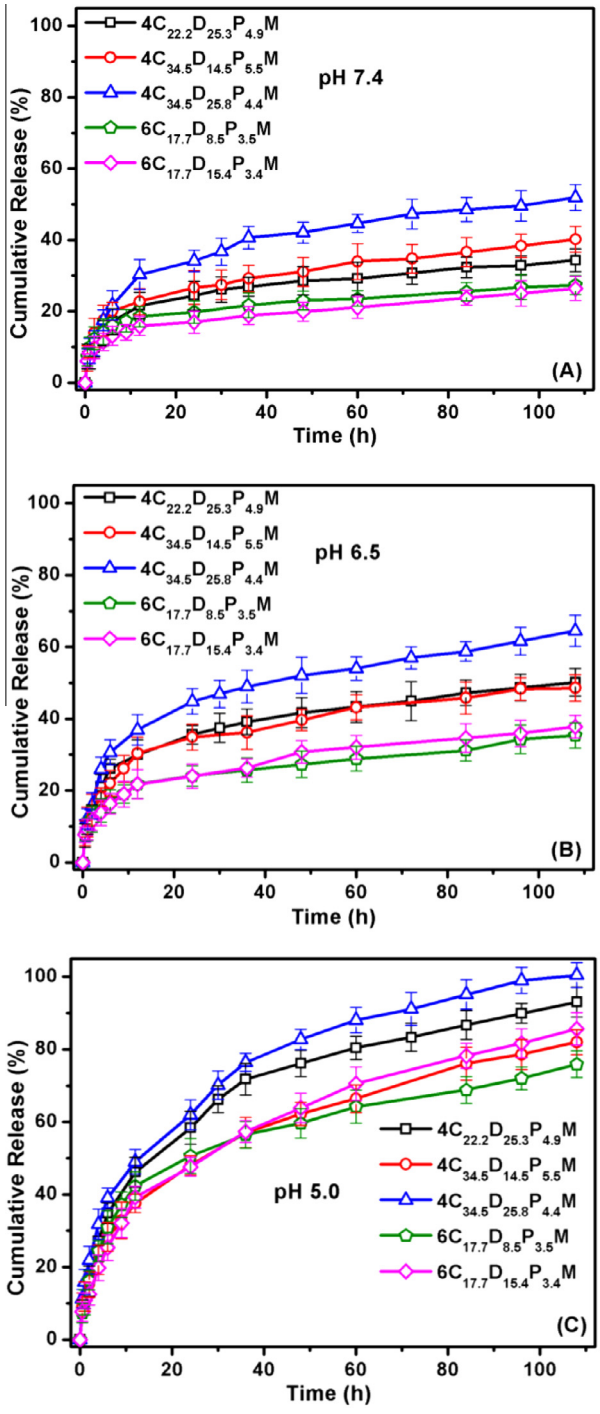

Fig. 4. In vitro drug release profiles of DOX-loaded 4AS-PCL-b-PDEAEMA-b-PPEGMA micelles under different pH conditions: (A) pH 7.4; (B) pH 6.5; (C) pH 5.0.

At pH 6.5 the release rates of DOX accelerated to a certain extent, as partial protonation of the tertiary amine groups of DEAEMA contributed to a slight swelling of the micelles. However, the relatively looser micelle structure could not promote a drastic increase in DOX release, with the cumulative release of DOX being increased byabout 5% in 12 h, 10% in 48 h, and 10–15% in 108 h, compared with pH 7.4, as shown in Fig. 4B. The release rate of DOX from $4C_{22.2}D_{25.3}P_{4.9}M$ was almost the same as that from $4C_{34.5}D_{14.5}P_{5.5}M$ at pH 6.5, which is slower at pH 7.4 compared with $4C_{34.5}D_{14.5}P_{5.5}M$, confirming that protonation of the tertiary amine groups of DEAEMA promoted the release of DOX.

Under more acidic conditions (pH 5.0) the release rates of DOX were drastically accelerated, without an obvious burst release, as shown in Fig. 4C. As most of the tertiary amine groups of DEAEMA were protonated, the distinctly decreased hydrophobicity of the micellar core and greatly increased electrostatic repulsion between DEAEMA moieties contributed to a greater degree of swelling or even a slight dissociation of micelles, and the entrapped DOX could be released at an accelerated rate. In addition, as the 4/6AS-PCL-b-PDEAEMA-b-PPEGMA micelles were designed as three layer structures protonation of the PDEAEMA chains could cause transformation of the micelle structure from compact three layer to loose two layer, altering the drug release profiles.

The in vitro drug release profiles can also be explained by coarse grained simulations of 4AS-PCL-b-PDEAEMA-b-PPEGMA micelles using the DPD method. Fig. 5 shows sections of DOX-loaded micelles at different pH values. At pH > 7.4 the outer PPEGMA around the core formed by PCL produced a spherical core–shell structure. The pH-sensitive PDEAEMA chains, mostly distributed between the core and the shell, are neither hydrated nor protonated, and the PDEAEMA layer is in a non-swollen state. DOX disperses into the PCL core and PDEAEMA layer. On decreasing the pH down to 6.5 the PDEAEMA chains become protonated, resulting in "cracks" on the surface of the PEG shell and the formation of water channels, which extrude PDEAEMA chains into the medium, resulting in DOX outward diffusion. Under lower pH (pH 5.0) conditions the structure of the micelles is swollen, resulting in more "cracks" and channels facilitating the release of DOX. It should be noted that the results of the DPD simulations are in accordance with the experimental results.

It can be seen that the length of the PDEAEMA block had a significant influence on the release of DOX. The cumulative release of DOX from $4C_{34.5}D_{25.8}P_{4.4}M$ was 50% in 12 h, 83% in 48 h, and 99% in 96 h, which is higher than 37% in 12 h, 62% in 48 h, and 78% in 96 h for $4C_{34.5}D_{14.5}P_{5.5}M$. The same tendency was observed for DOX release from $6C_{17.7}D_{8.5}P_{3.5}M$ and $6C_{17.7}D_{15.4}P_{3.4}M$, in that the cumulative – release of DOX was about 10% higher during the whole release process for the latter. The higher cumulative release of DOX from 4/6AS-PCL-b-PDEAEMA-b-PPEGMA micelles with longer PDEAEMA block lengths suggests that the sensitivity of the micellar core to pH change was enhanced and the burst release behavior was effectively restricted for the three layer structure micelles. The pH-sensitive release profiles conformed to the demands of anticancer drug administration, providing less leakage in normal tissues

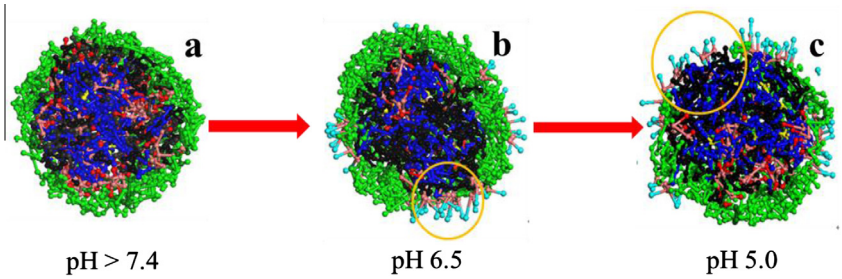

Fig. 5. Typical simulated section views of DOX-loaded 4AS-PCL-b-PDEAEMA-b-PPEGMA micelles under different pH conditions: (a) pH > 7.4; (b) pH 6.5; (c) pH 5.0.

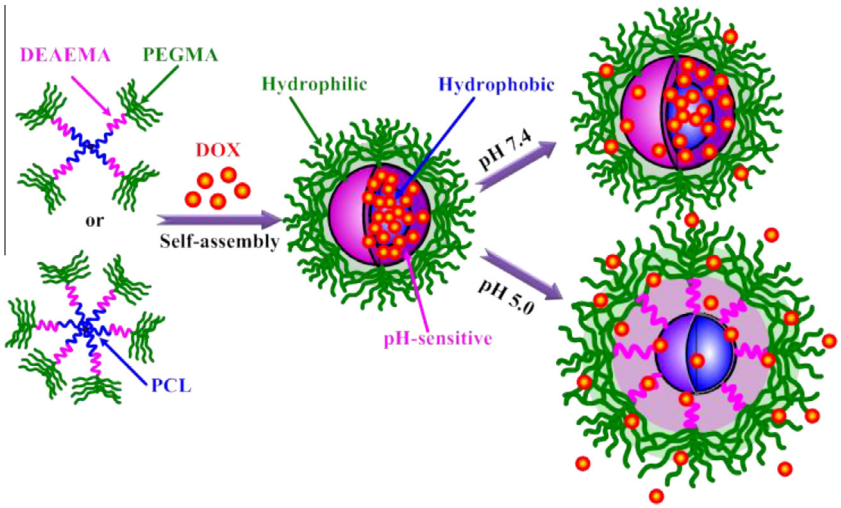

Fig. 6. Scheme of drug loading and pH-dependent release from 4AS-PCL-b-PDEAEMA-b-PPEGMA micelles.

and accelerated release in tumor cells (endosomal and lysosomal). Fig. 6 shows the schematic micellization of and pH-dependent drug release by 4/6AS-PCL-b-PDEAEMA-b-PPEGMA. The overall in vitro drug release results demonstrated that pH-responsive three layer micelles self-assembled from 4/6AS-PCL-b-PDEAEMA-b-PPEGMA can potentially be used as a promising vehicle for delivery of hydrophobic drugs with sustained release.

Although the mechanism of drug release from polymeric matrices is very complex and is still not completely understood, it can be simplistically classified as either pure diffusion, erosion controlled release or a combination of the two mechanisms [59]. The semi-empirical Eq. (3) of Ritger and Peppas [60] is widely applied for approximate analysis of the mechanism of drug release from polymeric matrices [61,62].

$$\log\left(\frac{M_t}{M_\infty}\right) = n\log t + \log k \tag{3}$$

where M_t and M_∞ are the absolute cumulative amounts of drug released at time t and infinite time, respectively, n is the release exponent indicating the drug release mechanism and k is a constant incorporating the structural and geometric characteristics of the device. For spherical particles the value of n is 0.43 for Fickian diffusion and 0.85 for a non-Fickian mechanism, $n < 0.43$ corresponds to a combination of diffusion and erosion control, and $0.43 < n < 0.85$ represents the anomalous transport mechanism [63]. Based on the above theory the in vitro DOX release data for pH 7.4, 6.5 and 5.0 were fitted to theoretical release profiles given by Eq. (3), as shown in Fig. 7.

It can be seen that the release of DOX from 4/6AS-PCL-b-PDEAEMA-b-PPEGMA micelles under all pH conditions could be divided into two stages with good linearity. The first stage is from 0 to 12 h and the second stage from 12 to 108 h. The fitting parameters, including the release exponent n, rate constant k, and the correlation coefficient R^2, are tabulated in Tables 4 and S1. At pH 7.4, shown in Table S1, the n values in the first stage were lower than 0.43, except for $4C_{34.5}D_{25.8}P_{4.4}M$, indicating that DOX release in the first 12 h corresponded to a combination of diffusion and erosion control. As most of the PDEAEMA was deprotonated and the micelle structure was tight diffusion of drug through the micellar core was difficult and bulk erosion played an important role in drug release. However, the n value of $4C_{34.5}D_{25.8}P_{4.4}M$ was 0.48, indicating that DOX release corresponded to the Fickian diffusion model. This could be attributed to the longer lengths of the PCL and PDEAEMA blocks in $4C_{34.5}D_{25.8}P_{4.4}M$, which led to mild swelling of the micelle core and DOX release controlled by diffusion. In the second stage the n values showed the same release behavior as in the first stage but the k values were higher, suggesting that the release rate accelerated with time.

As partial protonation of the tertiary amine groups of DEAEMA contributed to the slight swelling of the micelle structure at pH 6.5 drug release from 4AS-PCL-b-PDEAEMA-b-PPEGMA micelles was mainly controlled by diffusion, as the n values were close to 0.43, as tabulated in Table S1. However, the structure of the 6AS-PCL-b-PDEAEMA-b-PPEGMA micelles was compact and could not swell to a loose state at pH 6.5, and release of the drug was still controlled by the combination of diffusion and erosion. After 12 h, similarly to pH 7.4, drug release was controlled by a combination of polymer degradation and diffusion.

At pH 5.0, as shown in Table 4, as most of the tertiary amine groups of DEAEMA were protonated and the micelles had swollen to greater degree of loose structure, or even slight dissociation,

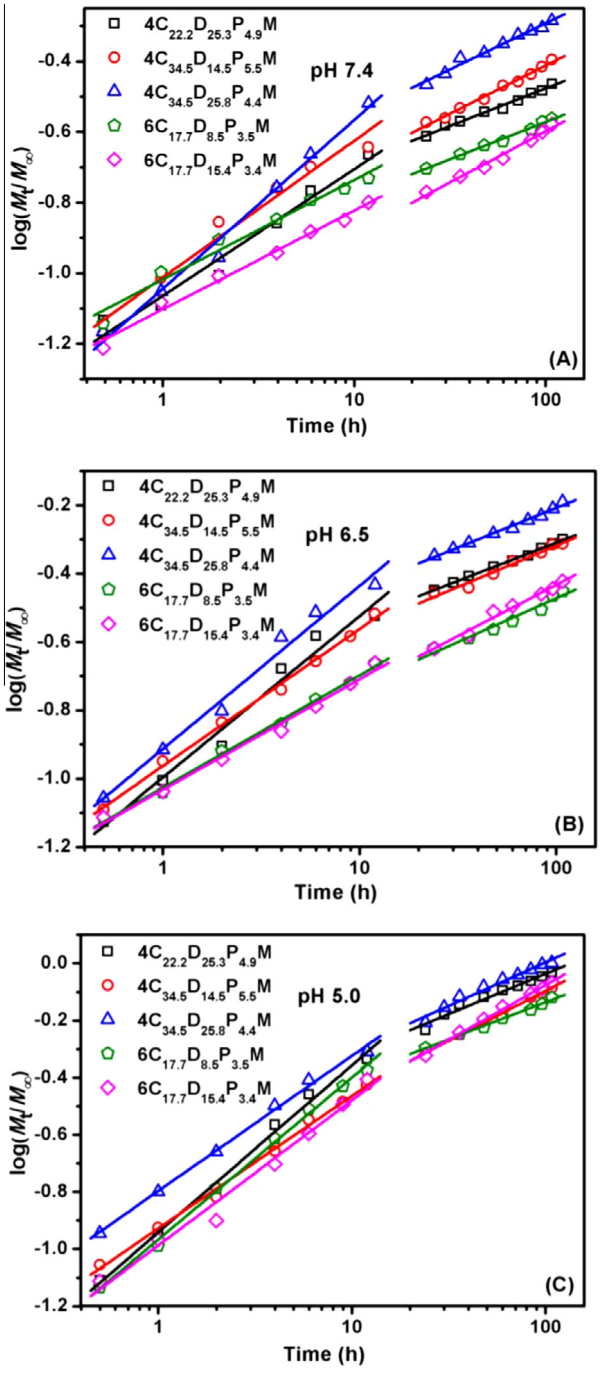

Fig. 7. Plots of $\log(M_t/M_\infty)$ against log time for DOX release from 4AS-PCL-b-PDEAEMA-b-PPEGMA micelles under different pH conditions: (A) pH 7.4; (B) pH 6.5 and (C) pH 5.0.

Table 4
Fitting parameters of in vitro DOX release data from 4AS-PCL-b-PDEAEMA-b-PPEGMA micelles at pH 5.0.

Matrix	n_1[a]	k_1[a]	R^2_1	n_2[b]	k_2[b]	R^2_2
$4C_{22.2}D_{25.3}P_{4.9}M$	0.58	0.11	0.992	0.28	0.25	0.968
$4C_{34.5}D_{14.5}P_{5.5}M$	0.46	0.12	0.995	0.35	0.16	0.996
$4C_{34.5}D_{25.8}P_{4.4}M$	0.47	0.16	0.995	0.30	0.25	0.970
$6C_{17.7}D_{8.5}P_{3.5}M$	0.57	0.11	0.997	0.26	0.22	0.992
$6C_{17.7}D_{15.4}P_{3.4}M$	0.51	0.10	0.979	0.38	0.14	0.994

[a] The first stage is 0–12 h.
[b] The second stage is 12–108 h.

DOX release from all the 4/6AS-PCL-b-PDEAEMA-b-PPEGMA micelles was mainly by Fickian diffusion and the n values of the first stage were close to 0.43. After 12 h the micelles reached a steady swollen state and DOX release was mainly by a combination of diffusion and erosion. The k values of the second stage were even higher than for pH 7.4 and 6.5, suggesting that the release rates accelerated with decreasing pH. Moreover, the k values of $4C_{34.5}D_{25.8}P_{4.4}M$ were higher compared with the other micelles under every pH condition, owing to the structural advantage of longer PCL and PDEAEMA block lengths.

As an overall result, the rates of DOX release from 4/6AS-PCL-b-PDEAEMA-b-PPEGMA micelles increased significantly as the PDEAEMA content was increased and the pH decreased. The DOX-loaded micelles gradually swelled resulting in a certain degree of loose structure with decreasing medium pH and the mechanism of DOX changed from a combination of diffusion and erosion control (pH 7.4) to steady diffusion (pH 5.0) in the first 12 h. Then the micelle began to dissociate or degrade and drug release was controlled by an interaction of diffusion and erosion in the second stage.

3.5. Cytotoxicity of DOX-loaded 4/6AS-PCL-b-PDEAEMA-b-PPEGMA micelles

The in vitro cytotoxicity of free DOX and blank and DOX-loaded micelles were investigated by MTT assay conducted in HepG2 (hepatocellular carcinoma) cells [57,64,65]. The blank 4/6AS-PCL-b-PDEAEMA-b-PPEGMA micelles were used as negative controls and free DOX at different concentrations (0–20 mg l^{-1}) served as positive controls. As shown in Fig. 8A, no obvious cytotoxicity of blank 4/6AS-PCL-b-PDEAEMA-b-PPEGMA micelles was observed in HepG2 cells. The cytotoxicity increased slightly with increasing length of the PDEAEMA block and the concentration of micelles. However, the percentage of viable cells for blank 4/6AS-PCL-b-PDEAEMA-b-PPEGMA micelles at their highest concentration (400 mg l^{-1}) was still over 90% after 24 h incubation, suggesting excellent biocompatibility with HepG2 cells.

The MTT-based cytotoxic activities of free DOX and DOX-loaded 4/6AS-PCL-b-PDEAEMA-b-PPEGMA micelles were compared after 24 (Fig. 8B) and 48 h (Fig. 8C) incubation and the IC_{50} values of DOX, the concentration at which 50% of cells were killed in a given period, were obtained from the cell viability data and are listed in Table 5. It appears that free DOX had a more potent activity than DOX-loaded micelles after 24 h incubation, except for $4C_{34.5}D_{25.8}P_{4.4}M$. This might be because DOX release from the micelles was a sustained release process after internalization within cells and DOX-loaded micelles might not enter the nucleus as quickly as free DOX. The cytotoxicity of DOX-loaded 6AS-PCL-b-PDEAEMA-b-PPEGMA micelles was much lower than that of 4AS-PCL-b-PDEAEMA-b-PPEGMA micelles, for a relatively slower release rate of DOX. The IC_{50} values of DOX-loaded 6AS-PCL-b-PDEAEMA-b-PPEGMA micelles were even higher, at 7.6 and 3.9 mg l^{-1} for $6C_{17.7}D_{8.5}P_{3.5}M$ and $6C_{17.7}D_{15.4}P_{3.4}M$, respectively. On the other hand, the length of the PDEAEMA block had an important influence on internalization of the micelles and DOX release properties from the micelles, as the longer length of the PDEAEMA block resulting in a higher positive charge on the micelles, facilitating their cellular uptake and a higher release efficiency of DOX after internalization within cells. Thus it can seen that the IC_{50} values of DOX-loaded $4C_{34.5}D_{25.8}P_{4.4}M$ and $6C_{17.7}D_{15.4}P_{3.4}M$ were almost half of those of $4C_{34.5}D_{14.5}P_{5.5}M$ and $6C_{17.7}D_{8.5}P_{3.5}M$. It is noteworthy that the cytotoxicity of DOX-loaded $4C_{34.5}D_{25.8}P_{4.4}M$ was very close to free DOX after 24 h incubation, which indicates that it could be a perfect candidate for anticancer drug delivery.

As described above, although the cellular uptake of DOX-loaded 4/6AS-PCL-b-PDEAEMA-b-PPEGMA micelles within cells was

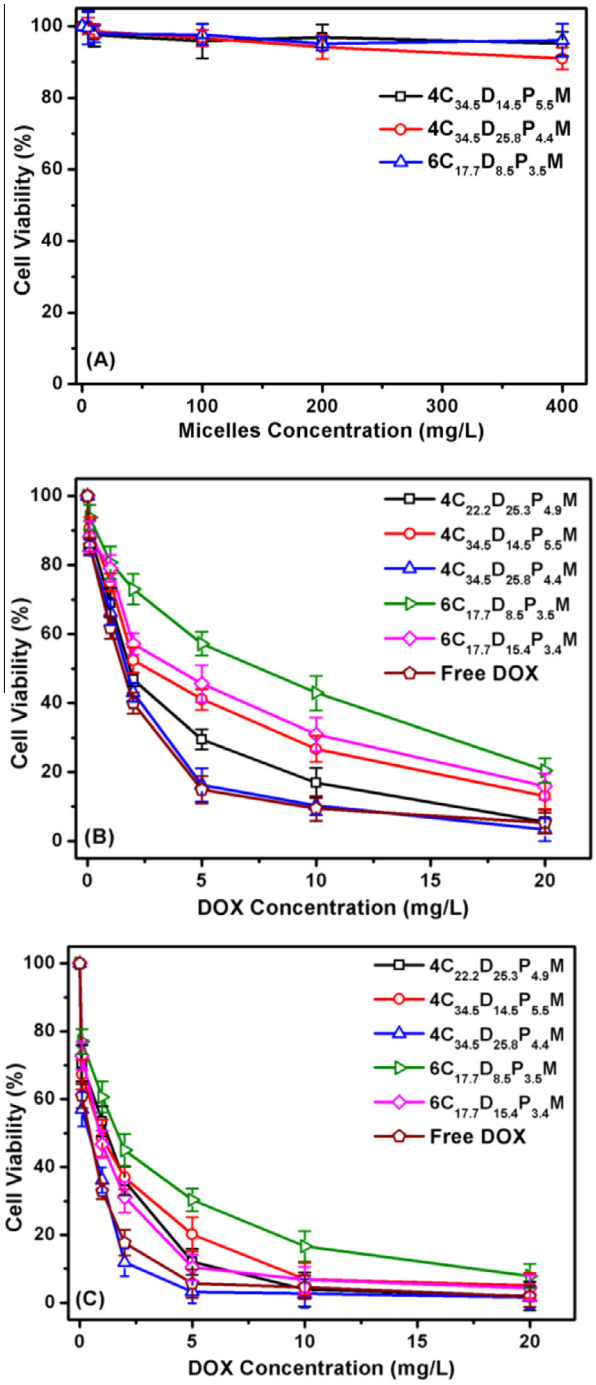

Fig. 8. The cytotoxicity to HepG2 cells of (A) blank 4/6AS-PCL-b-PDEAEMA-b-PPEGMA micelles after 24 h incubation at various polymer doses and free DOX or DOX-loaded 4AS-PCL-b-PDEAEMA-b-PPEGMA micelles after (B) 24 and (C) 48 h incubation at various DOX doses.

greater, DOX release from the micelles should proceed over a sustained period. Thus 48 h cell incubation was used in the viability assay. As shown in Fig. 8C, the cell viability and the IC_{50} values of the DOX-loaded 4/6AS-PCL-b-PDEAEMA-b-PPEGMA micelles were sharply decreased compared with 24 h. Possessing a longer length PDEAEMA block DOX-loaded $4C_{22.2}D_{25.3}P_{4.9}M$, $4C_{34.5}D_{25.8}P_{4.4}M$ and $6C_{17.7}D_{15.4}P_{3.4}M$ exhibited almost the same in vitro cytotoxicity as free DOX, which can be seen from the comparatively close IC_{50} values. Excitingly, it can be observed that DOX-loaded $4C_{34.5}D_{25.8}P_{4.4}M$ had the same IC_{50} value (0.5 mg l^{-1}) as free DOX and showed better cytotoxic activity than free DOX at concentrations over 2 mg l^{-1}, which suggests that $4C_{34.5}D_{25.8}P_{4.4}M$ could provide enhanced anticancer activity and bioavailability of DOX. Thus a lower dosage was needed for the same therapeutic efficacy [66].

Table 5
The IC_{50} values of DOX-loaded 4AS-PCL-b-PDEAEMA-b-PPEGMA micelles after 24 and 48 h incubation.

Sample	IC_{50} (mg l^{-1})	
	24 h	48 h
Free DOX	1.6 ± 0.021	0.5 ± 0.005
$4C_{22.2}D_{25.3}P_{4.9}M$	2.1 ± 0.024	1.2 ± 0.001
$4C_{34.5}D_{14.5}P_{5.5}M$	2.9 ± 0.031	1.0 ± 0.001
$4C_{34.5}D_{25.8}P_{4.4}M$	1.8 ± 0.012	0.5 ± 0.008
$6C_{17.7}D_{8.5}P_{3.5}M$	7.6 ± 0.043	1.8 ± 0.012
$6C_{17.7}D_{15.4}P_{3.4}M$	3.9 ± 0.035	0.9 ± 0.013

4. Conclusions

In the current work amphiphilic 4- and 6-armed star triblock co-polymers 4/6AS-PCL-b-PDEAEMA-b-PPEGMA and their self-assembled three layer micelles were developed for controlled delivery of hydrophobic anticancer drugs. The polymers showed extremely low CMC values which could markedly improve micelle stability and extend the range of applications in controlled drug delivery. The average sizes of the DOX-incorporating micelles were 120–230 nm, with a spherical shape. The in vitro release of DOX from the three layer micelles exhibited the desired pH-dependence owing to protonation of the tertiary amine groups of DEAEMA in the middle layer of the micelles. The DOX release rate was significantly accelerated by decreasing the pH from 7.4 to 5.0, which is closely related to the PCL and PDEAEMA contents and the topological structures of the polymers. The in vitro cytotoxicity of DOX-loaded micelles to HepG2 cells suggests that the 4/6AS-PCL-b-PDEAEMA-b-PPEGMA micelles could provide equivalent or even enhanced anticancer activity and bioavailability of DOX and thus a lower dosage was sufficient for the same therapeutic efficacy. The characteristics demonstrate that these micelles could have significant potential in anticancer drug delivery applications.

Acknowledgements

This work was financially supported by the National Natural Science Foundation of China (Grants nos. 21176090 and 21206045), Team Project of Natural Science Foundation of Guangdong Province, China (Grant S2011030001366), Project of International Cooperation and Exchanges of Guangdong Province, China (Grant 2011B050400016) and the Research Fund for the Doctoral Program of Higher Education of China (Grant 20110172120013).

Appendix A. Figures with essential colour discrimination

Certain figures in this article, particularly Figures 1–8, are difficult to interpret in black and white. The full colour images can be found in the on-line version, at http://dx.doi.org/10.1016/j.actbio.2013.05.006.

Appendix B. Supplementary data

Supplementary data associated with this article can be found, in the online version, at http://dx.doi.org/10.1016/j.actbio.2013.05.006.

References

[1] Lee ES, Gao ZG, Bae YH. Recent progress in tumor pH targeting nanotechnology. J Control Release 2008;132(3):164–70.
[2] Li X, Qian Y, Liu T, Hu X, Zhang G, You Y, et al. Amphiphilic multiarm star block copolymer-based multifunctional unimolecular micelles for cancer targeted drug delivery and MR imaging. Biomaterials 2011;32(27):6595–605.
[3] Kim S, Kim JY, Huh KM, Acharya G, Park K. Hydrotropic polymer micelles containing acrylic acid moieties for oral delivery of paclitaxel. J Control Release 2008;132(3):222–9.
[4] Torchilin V. Multifunctional and stimuli-sensitive pharmaceutical nanocarriers. Eur J Pharm Biopharm 2009;71(3):431–44.
[5] Wang WW, Deng LD, Liu SS, Li X, Zhao XM, Hu RJ, et al. Adjustable degradation and drug release of a thermosensitive hydrogel based on a pendant cyclic ether modified poly(-caprolactone) and poly(ethylene glycol)co-polymer. Acta Biomater 2012;8(11):3963–73.
[6] Petit A, Müller B, Bruin P, Meyboom R, Piest M, Kroon-Batenburg LMJ, et al. Modulating rheological and degradation pr operties of temperature-responsive gelling systems composed of blends of PCLA–PEG–PCLA triblock copolymers and their fully hexanoyl-capped derivatives. Acta Biomater 2012;8(12):4260–7.
[7] Zhang CY, Yang YQ, Huang TX, Zhao B, Guo XD, Wang JF, et al. Self-assembled pH-responsive MPEG-*b*-(PLA-*co*-PAE) block copolymer micelles for anticancer drug delivery. Biomaterials 2012;33(26):6273–83.
[8] Bastakoti BP, Guragain S, Yokoyama Y, Yusa S, Nakashim K. Incorporation and release behavior of amitriptylene in core–shell–corona type triblock copolymer micelles. Colloid Surf B Biointerfaces 2011;88:734–40.
[9] Liang YH, Liu CH, Liao SH, Lin YY, Tang HW, Liu SY, et al. Cosynthesis of cargo-loaded hydroxyapatite/alginate core–shell nanoparticles (HAP@Alg) as pH-responsive nanovehicles by a pregel method. ACS Appl Mater Interfaces 2012;4(12):6720–7.
[10] Tang SH, Huang XQ, Chen XL, Zheng NF. Hollow mesoporous zirconia nanocapsules for drug delivery. Adv Funct Mater 2010;20(15):2442–7.
[11] Wu KCW, Yang YH, Liang YH, Chen HY, Sung E, Yamauchi Y, et al. Facile synthesis of hollow mesoporous hydroxyapatite nanoparticles for intracellular bio-imaging. Curr Nanosci 2011;7(6):926–31.
[12] Lian HY, Hu M, Liu CH, Yamauchi Y, Wu KCW. Highly biocompatible, hollow coordination polymer nanoparticles as cisplatin carriers for efficient intracellular drug delivery. Chem Commun 2012;48(12):5151–3.
[13] Bastakoti BP, Inuoe M, Yusa S, Liao SH, Wu KCW, Nakashima K, et al. A block copolymer micelle template for synthesis of hollow calcium phosphate nanospheres with excellent biocompatibility. Chem Commun 2012;48(52):6532–4.
[14] Yang YQ, Guo XD, Lin WJ, Zhang LJ, Zhang CY, Qian Y. Amphiphilic copolymer brush with random pH-sensitive/hydrophobic structure: synthesis and self-assembled micelles for sustained drug delivery. Soft Matter 2012;8(2):454–64.
[15] Oerlemans C, Bult W, Bos M, Storm G, Nijsen JFW, Hennink WE. Polymeric micelles in anticancer therapy: targeting, imaging and triggered release. Pharm Res 2010;27(12):2569–89.
[16] GuoQ Cai, Zhang HW, Liu P, Wang LQ, Jiang HL. Triggered disassembly of hierarchically assembled onion-like micelles into the pristine core–shell micelles via a small change in pH. Acta Biomater 2011;7(10):3729–37.
[17] Xiong XB, Binkhathlan Z, Molavi O, Lavasanifar A. Amphiphilic block co-polymers: preparation and application in nanodrug and gene delivery. Acta Biomater 2012;8(6):2017–33.
[18] Zhu J, Zhou Z, Yang C, Kong D, Wan Y, Wang Z. Folate-conjugated amphiphilic star-shaped block copolymers as targeted nanocarriers. J Biomed Mater Res A 2011;97A(4):498–508.
[19] Prabaharan M, Grailer JJ, Pilla S, Steeber DA, Gong S. Amphiphilic multi-arm-block copolymer conjugated with doxorubicin via pH-sensitive hydrazone bond for tumor-targeted drug delivery. Biomaterials 2009;30(29):5757–66.
[20] Khanna K, Varshney S, Kakkar A. Miktoarm star polymers: advances in synthesis, self-assembly, and applications. Polym Chem 2010;1(8):1171–85.
[21] Wang Y, Grayson SM. Approaches for the preparation of non-linear amphiphilic polymers and their applications to drug delivery. Adv Drug Del Rev 2012;64(9):852–65.
[22] Triftaridou AI, Vamvakaki M, Patrickios CS, Stavrouli N, Tsitsilianis C. Synthesis of amphiphilic $(ABC)_n$ multiarm star triblock terpolymers. Macromolecules 2005;38(3):1021–4.
[23] Stavrouli N, Triftaridou AI, Patrickios CS, Tsitsilianis C. Multi-compartment unimolecular micelles from (ABC)n multi-arm star triblock terpolymers. Macromol Rapid Commun 2007;28(5):560–6.
[24] Yan YS, We DX, Li JY, Zheng JH, Shi GG, Luo WH, et al. A poly(l-lysine)-based hydrophilic star block co-polymer as a protein nanocarrier with facile encapsulation and pH-responsive release. Acta Biomater 2012;8(6):2113–20.
[25] Cajot S, Butsele KV, Paillard A, Passirani C, Garcion E, Benoit JP, et al. Smart nanocarriers for pH-triggered targeting and release of hydrophobic drugs. Acta Biomater 2012;8(12):4215–23.
[26] Xiao Y, Hong H, Javadi A, Engle JW, Xu W, Yang Y, et al. Multifunctional unimolecular micelles for cancer-targeted drug delivery and positron emission tomography imaging. Biomaterials 2012;33(11):3071–82.
[27] Zhou Y, Huang W, Liu J, Zhu X, Yan D. Self-assembly of hyperbranched polymers and its biomedical applications. Adv Mater 2010;22(41):4567–90.
[28] Ren TB, Wang, Yuan WZ, Li L, Feng Y. Synthesis, self-assembly, fluorescence, and thermosensitive properties of star-shaped amphiphilic copolymers with porphyrin core. J Polym Sci A Polym Chem 2011;49(10):2303–13.
[29] Knop K, Pavlov GM, Rudolph T, Martin K, Pretzel D, Jahn BO, et al. Amphiphilic star-shaped block copolymers as unimolecular drug delivery systems: investigations using a novel fungicide. Soft Matter 2013;9(3):715–26.
[30] Aryal S, Hu C-MJ, Zhang L. Polymer–cisplatin conjugate nanoparticles for acid-responsive drug delivery. ACS Nano 2009;4(1):251–8.
[31] Wang W, Cheng D, Gong F, Miao X, Shuai X. Design of multifunctional micelle for tumor-targeted intracellular drug release and fluorescent imaging. Adv Mater 2012;24(1):115–20.
[32] Zhao B-X, Zhao Y, Huang Y, Luo L-M, Song P, Wang X, et al. The efficiency of tumor-specific pH-responsive peptide-modified polymeric micelles containing paclitaxel. Biomaterials 2012;33(8):2508–20.
[33] Gao GH, Im GH, Kim MS, Lee JW, Yang J, Jeon H, et al. Magnetite-nanoparticle-encapsulated pH-responsive polymeric micelle as an MRI probe for detecting acidic pathologic areas. Small 2010;6(11):1201–4.
[34] Shen YQ, Zhan YH, Tang JB, Xu PS, Johnson PA, Radosz M, et al. Multifunctioning pH-responsive nanoparticles from hierarchical self-assembly of polymer brush for cancer drug delivery. AIChE J 2008;54(11):2979–89.
[35] Yu H, Zou Y, Wang Y, Huang X, Huang G, Sumer BD, et al. Overcoming endosomal barrier by amphotericin B-loaded dual pH-responsive PDMA-b-PDPA micelleplexes for siRNA delivery. ACS Nano 2011;5(11):9246–55.
[36] Min KH, Kim J-H, Bae SM, Shin H, Kim MS, Park S, et al. Tumoral acidic pH-responsive MPEG-poly(β-amino ester) polymeric micelles for cancer targeting therapy. J Control Release 2010;144(2):259–66.
[37] Liu H, Li CH, Liu HW, Liu SY. PH-responsive supramolecular self-assembly of well-defined zwitterionic ABC miktoarm star terpolymers. Langmuir 2009;25(8):4724–34.
[38] He E, Ravi P, Tam KC. Synthesis and self-assembly behavior of four-arm poly(ethylene oxide)-b-poly(2-(diethylamino)ethyl methacrylate) star block copolymer in salt solutions. Langmuir 2007;23(5):2382–8.
[39] He E, Yue CY, Simeon F, Zhou LH, Too HP, Tam KC. Polyplex formation between four-arm poly(ethylene oxide)-b-poly(2-(diethylamino)ethyl methacrylate) and plasmid DNA in gene delivery. J Biomed Mater Res A 2009;91A(3):708–18.
[40] Huang X, Xiao Y, Lang M. Self-assembly of pH-sensitive mixed micelles based on linear and star copolymers for drug delivery. J Colloid Interface Sci 2011;364(1):92–9.
[41] Cao W, Zhou J, Wang Y, Zhu L. Synthesis and in vitro cancer cell targeting of folate-functionalized biodegradable amphiphilic dendrimer-like star polymers. Biomacromolecules 2010;11(12):3680–7.
[42] Hussain H, Mya KY, He CB. Self-assembly of brush-like poly[poly(ethylene glycol) methyl ether methacrylate] synthesized via aqueous atom transfer radical polymerization. Langmuir 2008;24(23):13279–86.
[43] Weaver JVM, Williams RT, Royles BJL, Findlay PH, Cooper AI, Rannard SP. PH-responsive branched polymer nanoparticles. Soft Matter 2008;4(5):985–92.
[44] Chen T, Shukoor MI, Wang R, Zhao Z, Yuan Q, Bamrungsap S, et al. Smart multifunctional nanostructure for targeted cancer chemotherapy and magnetic resonance imaging. ACS Nano 2011;5(10):7866–73.
[45] Guo XD, Zhang LJ, Wu ZM, Qian Y. Dissipative particle dynamics studies on microstructure of pH-sensitive micelles for sustained drug delivery. Macromolecules 2010;43(18):7839–44.
[46] Li YM, Xu GY, Luan YX, Yuan SL, Zhang ZQ. Studies on the interaction between tetradecyl dimethyl betaine and sodium carboxymethyl cellulose by DPD simulations. Colloid Surf A 2005;257:385–90.
[47] Peng C-L, Shieh M-J, Tsai M-H, Chang C-C, Lai P-S. Self-assembled star-shaped chlorin-core poly(-caprolactone)–poly(ethylene glycol) diblock copolymer micelles for dual chemo-photodynamic therapies. Biomaterials 2008;29(26):3599–608.
[48] Schramm OG, Pavlov GM, van Erp HP, Meier MAR, Hoogenboom R, Schubert US. A versatile approach to unimolecular water-soluble carriers: ATRP of PEGMA with hydrophobic star-shaped polymeric core molecules as an alternative for PEGylation. Macromolecules 2009;42(6):1808–16.
[49] Jakubowski W, Matyjaszewski K. Activators regenerated by electron transfer for atom-transfer radical polymerization of (meth)acrylates and related block copolymers. Angew Chem Int Ed 2006;45(27):4482–6.
[50] Pasquale AJ, Long TE. Synthesis of star-shaped polystyrenes via nitroxide-mediated stable free-radical polymerization. J Polym Sci A Polym Chem 2001;39(1):216–23.
[51] Pasquale AJ, Long TE. Real-time monitoring of the stable free radical polymerization of styrene via in-situ mid-infrared spectroscopy. Macromolecules 1999;32(23):7954–7.
[52] Zhang LY, Guo R, Yang M, Jiang XQ, Liu BR. Thermo and pH dual-responsive nanoparticles for anti-cancer drug delivery. Adv Mater 2007;19(19):2988–92.
[53] Yang YQ, Zheng LS, Guo XD, Qian Y, Zhang LJ. PH-sensitive micelles self-assembled from amphiphilic copolymer brush for delivery of poorly water-soluble drugs. Biomacromolecules 2010;12(1):116–22.
[54] Lele BS, Leroux JC. Synthesis and micellar characterization of novel amphiphilic A-B–A triblock copolymers of *N*-(2-hydroxypropyl)methacrylamide or *N*-vinyl-2-pyrrolidone with poly(ε-caprolactone). Macromolecules 2002;35(17):6714–23.
[55] Hong HY, Mai YY, Zhou YF, Yan DY, Cui J. Self-assembly of large multimolecular micelles from hyperbranched star copolymers. Macromol Rapid Commun 2007;28(5):591–6.

[56] Guo XD, Tandiono F, Wiradharma N, Khor D, Tan CG, Khan M, et al. Cationic micelles self-assembled from cholesterol-conjugated oligopeptides as an efficient gene delivery vector. Biomaterials 2008;29(36):4838–46.
[57] Guo XD, Zhang LJ, Chen Y, Qian Y. Core/shell pH-sensitive micelles self-assembled from cholesterol conjugated oligopeptides for anticancer drug delivery. AIChE J 2010;56(7):1922–31.
[58] Sant VP, Smith D, Leroux JC. Novel pH-sensitive supramolecular assemblies for oral delivery of poorly water soluble drugs: preparation and characterization. J Control Release 2004;97(2):301–12.
[59] Young CR, Dietzsch C, Cerea M, Farrell T, Fegely KA, Rajabi-Siahboomi A, et al. Physicochemical characterization and mechanisms of release of theophylline from melt-extruded dosage forms based on a methacrylic acid copolymer. Int J Pharm 2005;301(1/2):112–20.
[60] Ritger PL, Peppas NA. A simple equation for description of solute release I. Fickian and non-fickian release from non-swellable devices in the form of slabs, spheres, cylinders or discs. J Control Release 1987;5(1):23–36.
[61] Siepmann J, Göpferich A. Mathematical modeling of bioerodible, polymeric drug delivery systems. Adv Drug Del Rev 2001;48(2/3):229–47.
[62] Siepmann J, Peppas NA. Modeling of drug release from delivery systems based on hydroxypropyl methylcellulose (HPMC). Adv Drug Del Rev 2001;48(2/3):139–57.
[63] Li Y, Li H, Wei M, Lu J, Jin L. PH-responsive composite based on prednisone-block copolymer micelle intercalated inorganic layered matrix: structure and in vitro drug release. Chem Eng J 2009;151(1–3):359–66.
[64] Liu G, Jin Q, Liu X, Lv L, Chen C, Ji J. Biocompatible vesicles based on PEO-b-PMPC/α-cyclodextrin inclusion complexes for drug delivery. Soft Matter 2011;7(2):662–9.
[65] Yoo HS, Lee KH, Oh JE, Park TG. In vitro and in vivo anti-tumor activities of nanoparticles based on doxorubicin–PLGA conjugates. J Control Release 2000;68(3):419–31.
[66] Gao Y, Chen Y, Ji X, He X, Yin Q, Zhang Z, et al. Controlled intracellular release of doxorubicin in multidrug-resistant cancer cells by tuning the shell-pore sizes of mesoporous silica nanoparticles. ACS Nano 2011;5(12):9788–98.